

# Elimination of interface defects in mismatched epilayers by a reduction in growth area

E. A. Fitzgerald, P. D. Kirchner,<sup>a)</sup> R. Proano, G. D. Pettit,<sup>a)</sup> J. M. Woodall,<sup>a)</sup> and D. G. Ast

*Department of Materials Science and Engineering, Cornell University, Ithaca, New York 14853*

(Received 18 January 1988; accepted for publication 29 February 1988)

We have eliminated interface defects from the mismatched  $\text{In}_{0.05}\text{Ga}_{0.95}\text{As}/(001)\text{GaAs}$  interface by controlling the size of the growth area.  $2\text{-}\mu\text{m}$ -high pillars with different lateral shapes and dimensions were defined within the GaAs substrate before the molecular beam epitaxial growth of  $3500\text{ \AA}$  of  $\text{In}_{0.05}\text{Ga}_{0.95}\text{As}$ , greater than four times the critical thickness. On the pillars, the linear density of misfit dislocations was reduced from  $> 5000$  dislocations/cm for large (several hundred  $\mu\text{m}$  lateral dimensions) growth areas to nearly zero for  $25\text{ }\mu\text{m}$  lateral dimensions. The dislocation density remains less than 800 dislocations/cm for lateral dimensions up to  $100\text{ }\mu\text{m}$ . We find that there is also a decrease in dislocation density in narrow channels between the pillars; therefore, the pillars also block the glide of misfit dislocations.

Lattice-mismatched semiconductor systems have been extensively investigated for the realization of strained-layer devices. Promising devices have been fabricated with the  $\text{InGaAs}/\text{GaAs}$  system.<sup>1-3</sup> Employing higher In concentrations and thicker overlayers will improve device performance. In order to realize such devices, the misfit dislocations which form as a result of the lattice mismatch at high In concentrations or for large epilayer thicknesses must be eliminated. This can be achieved by preventing the nucleation of misfit dislocations, by minimizing dislocation multiplication, and limiting the glide of existing misfit dislocations. Possible nucleation mechanisms such as the glide of threading dislocations, multiplication of misfit dislocations, and the formation of surface dislocation half-loops have been discussed by Matthews *et al.*,<sup>4-6</sup> and dislocation multiplication has been discussed in detail by Hagen and Strunk.<sup>7</sup> Matthews *et al.* originally attributed the formation of misfit dislocations to the lateral glide of threading dislocations.<sup>4</sup> They point out that if threading dislocations were the source of misfit dislocations, one should be able to reduce the density of interface dislocations by limiting the lateral dimension of the sample before growth because too few threading dislocations would be present to nucleate a large number of misfit dislocations. However, it was observed that the number of misfit dislocations at the interface exceeded the number of misfit dislocations that could be generated from threading dislocations.<sup>5</sup> Hagen and Strunk proposed the interaction of misfit dislocations as an additional source of misfit dislocations,<sup>7</sup> and Matthews *et al.* considered the surface nucleation of dislocation half-loops to be a possible explanation for the observed dislocation density.<sup>5,6</sup>

We wish to point out that reducing the interface defect density by limiting the lateral dimension prior to growth should hold true for any nucleation sources that depend on area, such as dislocation interactions, particles, and threading dislocations, as long as the misfit is not large enough to generate other sources of misfit dislocations such as surface nucleation. If non-area-dependent nucleation sources do become active, the reduction of dislocation density with growth area will still be observed, but the lowest achievable

dislocation density will be higher than if these sources were not active.

To demonstrate this effect, we have fabricated  $2\text{-}\mu\text{m}$ -high pillars of GaAs on a (001) GaAs substrate. The substrate was patterned with photoresist, and electron beam evaporation was used to deposit  $\text{SiO}_x$  in a variety of lateral geometries (circles, squares, rectangles, and triangles) and dimensions ( $2\text{--}400\text{ }\mu\text{m}$ ). After removing the photoresist, the samples were then ion beam etched to form  $2\text{-}\mu\text{m}$ -deep trenches, producing pillars with very high aspect ratios. After we used a 10% HF acid and water solution to remove the  $\text{SiO}_x$  from the top of the pillars,  $200\text{ \AA}$  of GaAs were wet etched to remove any additional contamination. A  $1500\text{ \AA}$  buffer layer of GaAs was deposited by molecular beam epitaxy at  $550\text{ }^\circ\text{C}$ , followed by  $3500\text{ \AA}$  of  $\text{In}_{0.05}\text{Ga}_{0.95}\text{As}$ . All layers were doped with Si to  $10^{18}\text{ cm}^{-3}$  to increase the intensity of the cathodoluminescence (CL) signal. CL was used to determine the quality of the interface by imaging the dislocations in the interface plane. CL was also used to determine the substrate dislocation density. The dislocations in the substrate appear as black dots in the CL images. By counting these black dots, we arrive at a substrate dislocation density of  $1.5 \times 10^5\text{ cm}^{-2}$ .

To observe CL from the specimens, a JEOL JSM35CF scanning electron microscope was equipped with an annular Si photodiode<sup>8</sup> and a monochromator-photomultiplier detection system.<sup>9</sup> Electron beam x-ray analysis (utilizing wavelength dispersive spectroscopy) and wavelength-sensitive CL were used to analyze the In compositions on the top of the pillars. The composition was found to be  $\text{In}_{0.05}\text{Ga}_{0.95}\text{As}$  on all pillar structures and across the wafer. Rutherford backscattering spectrometry was used to confirm the  $3500\text{ \AA}$  epilayer thickness.

In this letter, data from the circular pillars will be discussed in detail. Figure 1(a) is a CL image of the  $\text{In}_{0.05}\text{Ga}_{0.95}\text{As}$  on GaAs without any lateral restriction (i.e.,  $> 1000\text{ }\mu\text{m}$ ). The  $15\text{ keV}$ ,  $80\text{ nA}$  electron beam was perpendicular to the interface plane. Defects appear as dark lines in the image because of a decrease in the amount of band-gap radiation emitted in the vicinity of the defect. There is such a high density of defects in Fig. 1(a) that we are not able to

<sup>a)</sup> IBM T. J. Watson Research Center, Yorktown Heights, NY 10598.

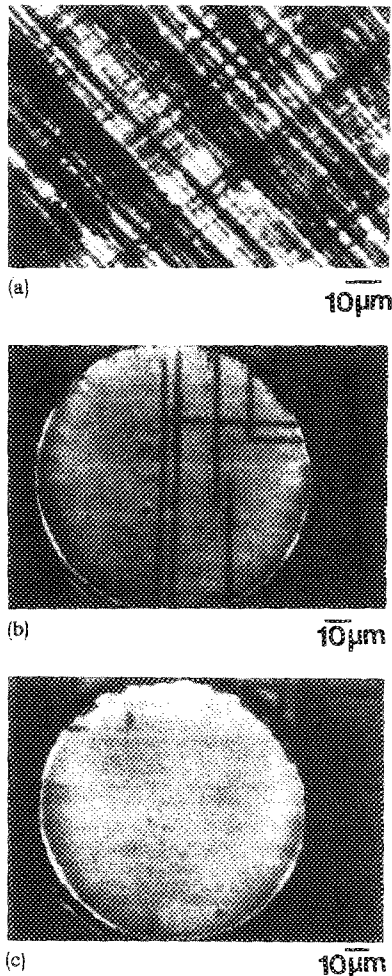


FIG. 1. CL images of the 3500 Å  $\text{In}_{0.05}\text{Ga}_{0.95}\text{As}$  layer on GaAs; (a) with no lateral restriction, (b) on a 90- $\mu\text{m}$ -diam pillar, and (c) on a 67  $\mu\text{m}$  pillar.

accurately determine the dislocation density due to the spatial resolution limit of the CL technique. In high defect density interfaces, the dislocation density is actually much higher than the dark-line defect density.<sup>9</sup> In Fig. 1(a), we can estimate from the dark-line defect density that the linear dislocation density is greater than 5000 dislocations/cm.

Figure 1(b) is a CL image of a circular pillar with a diameter of 90  $\mu\text{m}$ . On this pillar, the interface dislocation density is much lower than that seen in Fig. 1(a) for the large deposition area. The defect density is low enough so that each dark line corresponds to a single misfit dislocation.<sup>10</sup> By decreasing the lateral dimension further, we have eliminated the dislocations at the interface, as can be seen in Fig. 1(c), which is a 67- $\mu\text{m}$ -diam circular pillar. This effect is observed in other geometries as well, such as square and rectangular areas.

Figure 2 is a plot of the linear dislocation density along each  $\langle 110 \rangle$  direction versus the diameter of the circular pillars. For each pillar size, a number of pillars were analyzed and an average dislocation density was calculated. The figure clearly shows an asymmetry in dislocation density for the two  $\langle 110 \rangle$  directions. It is well known that misfit dislocations lying along the two  $\langle 110 \rangle$  directions in a (001) plane (termed  $\alpha$  and  $\beta$ ) have different structure<sup>11</sup> and mobility.<sup>12</sup>

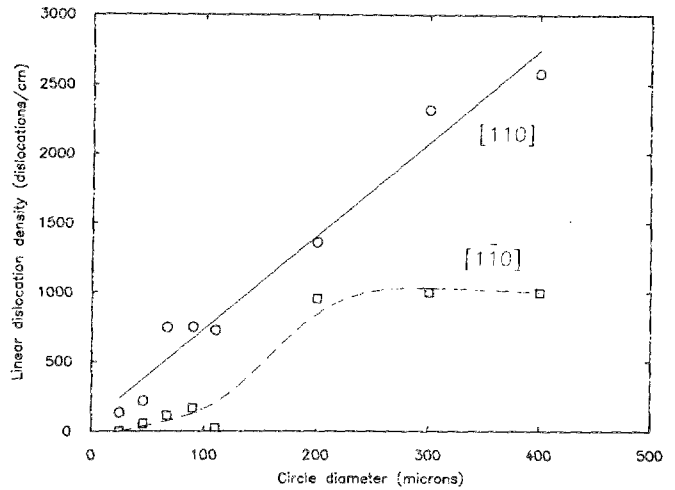


FIG. 2. Plot of linear dislocation density vs the diameter of the pillar for the two  $\langle 110 \rangle$  directions.

The  $\alpha$  dislocations have a higher dislocation mobility and lower activation energy than the  $\beta$  dislocations. The large asymmetry in the dislocation densities suggests that  $\alpha$  dislocations nucleate more readily than  $\beta$  dislocations. In Fig. 2 we have plotted an average linear dislocation density, but we point out that the smaller pillars ( $< 67 \mu\text{m}$ ) contain only 0–3 dislocations per pillar.

Different kinds of lateral dimension reduction decrease the dislocation density. In Fig. 3, a group of circular pillars is shown. Note that in addition to preventing dislocations from propagating on top of the pillars, the structures block dislocations in the interpillar background as well. This is most easily seen in the area between the circular pillars where the dislocations are all in one direction; i.e., gliding misfit dislocations are blocked by the pillars, and the area in between is not large enough to nucleate many misfit dislocations. Thus lateral restriction prior to growth, either by artificial islands or walls, will decrease the dislocation density.

When depositing epilayers on a large wafer, one has to contend with nucleation sites across an entire wafer; the nucleating dislocations can glide across the wafer area, resulting in a high dislocation density. Also, many dislocation interactions occur and result in additional misfit dislocations. The reduction in lateral dimension reduces the interface dislocation density by decreasing the number of active nucleation sites within that area and by preventing dislocation mul-

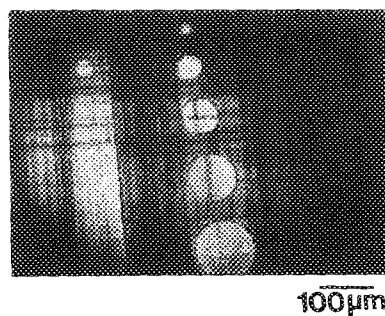


FIG. 3. CL image of a group of pillars which have prohibited the gliding of misfit dislocations.

tiplication by minimizing the distance a dislocation must travel to reach a free edge. If we assume that there are a number of fixed nucleation sites per unit area that are responsible for the area dependence of the linear dislocation density, and there is not any dislocation multiplication, then the slope of the [110] line in Fig. 2 implies a misfit dislocation nucleation site density of  $\approx 7 \times 10^4 - 1.4 \times 10^5 \text{ cm}^{-2}$ . Recall that the density of dislocations in the substrate was  $1.5 \times 10^7 \text{ cm}^{-2}$ , slightly greater than the calculated nucleation site density. But not all of the substrate threading dislocations counted are glissile  $60^\circ$  dislocations with Burgers vectors that can relieve stress at the interface. Therefore, the calculated density of nucleation sites using Fig. 2 suggests that threading dislocations are the primary source of misfit dislocations when other sources are inoperable. Also, because the [110] line in Fig. 2 nearly passes through zero, no other nucleation sites that are independent of area have become active.

We have shown that reducing the lateral dimension of the growth surface, prior to growth, can reduce the misfit dislocation density for  $3500 \text{ \AA}$   $\text{In}_{0.05}\text{Ga}_{0.95}\text{As}$  on (001) GaAs, which is greater than four times the previously accepted critical thickness. The dislocation density is reduced on the vertical structures as well as in between the structures. It is shown that one type of dislocation, presumably the more mobile  $\alpha$  dislocation, nucleates much more readily than the  $\beta$  dislocations. Further studies of the dependence of the interface defect density on the lateral growth area are expected to lead to an increased understanding of misfit dislocation nucleation as well as to the fabrication of previously unat-

tainable devices. Because the above technique is based upon fundamental properties of misfit dislocation nucleation, we expect that it is not limited to this material system.

We would like to thank Robert Davis for the chemically assisted ion beam etching and John Hunt for aiding in the microprobe analysis. We would like to acknowledge support from both the Department of Energy under contract No. DE-FG02-86ER45278 and the IBM fellowship program. The microscopy facility at Cornell University is operated by the Materials Science Center at Cornell University and supported through a National Science Foundation grant No. DMR85-16616-AO.

- <sup>1</sup>J. J. Rosenberg, M. Benlami, P. D. Kirchner, J. M. Woodall, and G. D. Petit, *IEEE Electron Device Lett.* **EDL-6**, 491 (1985).
- <sup>2</sup>L. P. Ramberg, P. M. Enquist, Y.-K. Chen, F. E. Najjar, L. F. Eastman, E. A. Fitzgerald, and K. L. Kavanagh, *J. Appl. Phys.* **61**, 1234 (1987).
- <sup>3</sup>S. Katsumoto, A. Yamamoto, and M. Yamaguchi, *Jpn. J. Appl. Phys.* **24**, 636 (1985).
- <sup>4</sup>J. W. Matthews, S. Mader, and T. B. Light, *J. Appl. Phys.* **41**, 3800 (1970).
- <sup>5</sup>J. W. Matthews, A. E. Blakeslee, and S. Mader, *Thin Solid Films* **33**, 253 (1976).
- <sup>6</sup>J. W. Matthews, *J. Vac. Sci. Technol.* **12**, 126 (1975).
- <sup>7</sup>W. Hagen and H. Strunk, *Appl. Phys.* **17**, 85 (1978).
- <sup>8</sup>J. Marek, R. Geiss, L. Glassman, and M. Scott, *J. Electrochem. Soc.* **132**, 1502 (1985).
- <sup>9</sup>E. A. Fitzgerald, D. G. Ast, P. D. Kirchner, G. D. Petit, and J. M. Woodall, *J. Appl. Phys.* **63**, 693 (1988).
- <sup>10</sup>E. A. Fitzgerald, Y. Ashizawa, L. F. Eastman, and D. G. Ast, *J. Appl. Phys.* (to be published).
- <sup>11</sup>M. S. Abrahams, J. Blanc, and C. J. Buiocchi, *Appl. Phys. Lett.* **21**, 185 (1972).
- <sup>12</sup>H. Steinhardt and P. Haasen, *Phys. Status Solidi A* **49**, 93 (1978).